Technical Issues on Static Load Tests on Barrettes and Bored Piles

K. Watanabe[1], T. Hosoi[2], S. Matsushita[3], A. S. Balasubramaniam[4], and R. N. Hwang[5]
[1]Geotechnical Engineering Department, Technical Research Institute, Obayashi Corporation, Research Engineer, Japan
[2]WSP Persons Brinckerhoff, Technical Advisor, Singapore
[3]Matsushita M&C Lab, Chief Engineer, Japan
[4]Griffith School of Engineering, Griffith University, Professor, Australia
[5]Moh and Associates, Inc., New Taipei City, Taiwan
E-mail: watanabe.koji.ro@obayashi.co.jp
E-mail: watakoji1128@gmail.com

ABSTRACT: This paper addresses to 1) Characteristic of slurry and mechanism of forming cakes, 2) Effects of the shapes of piles on load capacities, and 3) Modulus of elasticity of concrete. The results of laboratory tests on the strengths of mud cakes formed of bentonite slurry and polymer slurry are discussed. Also discussed are the results of loading tests on bored piles and barrettes with and with nodules. It has been found that the mud cakes formed of polymer slurry offer larger frictional resistance to shearing than bentonite slurry. It has also been found that nodules on piles will increase the load capacities of piles drastically. Furthermore, equations are proposed for calculating the moduli of elasticity of concrete based on the axial loads and stains obtained in pile load tests.

KEYWORDS: Slurry effect, Polymer slurry, Friction resistance, Cake, Slurry management, Shape effect, Non-uniform shaft pile, Under-reamed piles, Elastic modulus

1. INTRODUCTION

Barrettes and bored piles have been extensively adopted in lieu of precast piles nowadays to support structures because of the concern on noise and vibration during the installation of precast piles and also because of the large load capacities of barrettes and bored piles. Barrettes are rectangular piles installed by using the diaphragm walling technique. The term "barrette" is used interchangeably with "diaphragm wall" hereinafter, and is more preferred to diaphragm wall because the later usually refers to "walls" rather than "piles".

Over the past few decades, technology has advanced drastically on the design and construction of barrettes and bored piles as more and more experience is gained. In this paper, the following important aspects regarding the design and construction of barrettes and bored piles are discussed:

1) Effects of slurry on the bearing capacity of barrettes and bored piles with considerations given to the composition of slurry and the mechanism of cakes formation. In this regard, laboratory tests were conducted to study the performance of slurry and the results are discussed.
2) Shape effects on the bearing capacities of barrettes and bored piles. Pile load tests were conducted on barrettes and bored piles with and without nodules and the results are discussed.
3) Modulus of elasticity of cast-in-place concrete piles subjected to compressive and tensional loading.

2. EFFECTS OF SLURRY ON BEARING CAPACITIES OF BARRETTES AND BORED PILES

Bentonite slurry has been successfully used in underground works for more than sixty years. The rising cost of bentonite and the high transportation costs, however, have promoted the development of new types of colloidal materials, e.g, polymer slurry. Polymer slurry has now been widely used as an alternative to bentonite slurry in the USA and in Asia and is getting more and more popular in European countries.

2.1 Types and characteristics of polymers

Polymers which consist of water soluble macromolecules can generally be categorized as follows:

1) Biopolymer such as Chitosan, Xanthan gum, etc.
2) Semi-synthetic polymers, which are manufactured by conversion of natural macromolecules, such as Sodium Carboxyl Methyl Cellulose (CMC).
3) Fully synthetic polymers such as PHPA (partially Hydrolyzed Polyacrylamide).

Japan is one of the first countries to adopt polymer slurry for foundation works (Carlos, L. and Stephan, A. J., 2014). As early as 1973, biopolymer "Telmarch" and semi-synthetic polymer "OP-4" started to be used in Japan for installing deep foundations and diaphragm walls. The use of Telmarch was highly successful in the early days, however gradually declined because of the bio-degradation of biopolymer. It has now been totally abandoned in practice.

In contrast, CMC polymer slurry was specified in 1983 by the Japan National Railroad for Nagoya Station of Subway Line 6 Project and has been dominantly adopted in underground works in Japan and Asian countries since then. In the early stage of its application, CMC (OP-4) had degrees of substitution (D.S.) less than 1.0 and was susceptible to biodegradation. It has now been improved to increase the tolerance to bio-degradation and salt to 1.3 to 1.5 D.S.

Full synthetic polymer has been used mainly in the USA as slurry suspensions for deep boring. For example, PHAP has been adopted for foundation works since the 1990s. Today the use of PHPA polymer fluids has already spread from North America to many other countries.

Polymer slurry has many benefits over the traditional bentonite slurry, including: compact descanting plant, higher frequency of recycling, less environmental impact, lower construction cost (with the cost of the disposal accounted for) and better performance, etc. However, the application of polymer slurry in deep foundations and diaphragm walls has not always been successful as problems might occur unexpectedly. For example, synthetic polymer, such as polyacrylamide, in contact with fine soil particles in the trench is likely to be adhered to soil particles and transported to the de-sanding plant together with these soil particles. The absorbed polymer is unable to be separated from these soil particles and will be disposed as spoils. Consequently, the concentration of the polymer in the trench is gradually reduced. On the other hand, polymer in contact with cement particles would flocculate and become ineffective. Therefore, the quality of the slurry must be constantly monitored and maintained to ensure the slurry to serve its purposes.

In some projects, mix of bentonite and polymer is used to take the advantages, and meanwhile to compensate the shortcomings, of both agents. Generally, mix with a bentonite/polymer ratio less than 10 is classified as "polymer slurry" and mix with a bentonite/polymer ratio more than 40 is classified as "bentonite slurry".

2.2 Frictional resistance of polymer slurry

Tests have been conducted to compare the strengths of cakes formed of bentonite slurry with those formed of polymer slurry. Figure 1 shows the test apparatus which was modified from the conventional box shear apparatus. Seventeen acrylic ring sheets (0.2 mm thick each) were laid on the shearing plane to obtain the smallest shear resistance mobilized between concrete and soil.

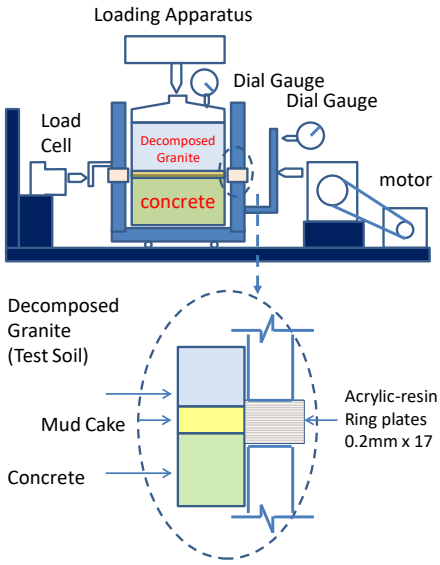

Figure 1 Slurry Test Apparatus (Hosoi 1993)

The compositions of the slurry tested are given in Table 1. The soil consists of decomposed granite with the following properties;

Internal friction angle: ϕ_d*=39.9 (deg.)*
Cohesion: c_d*=0 (kN/m*^{2}*)*
Unit weight: γ_t*=20kN/m*^{3}
Maximum and minimum void ratio: e_{max}*=0.88,* e_{min}*=0.59*
Average particle size: D_{50}*=1.41 (mm)*
Uniformity coefficient: D_{60}/D_{50}*=5.88.*

Table 1 Proportion of slurry tested (per 100cc of water)

Type of Slurry	Water (cc)	Bentonite (g)	Polymer (CMC) (g)	Distribution Agent (g)
Bentonite	100.0	6.0	0.1	0.2
Polymer	100.0	2.0	0.4	0.0

Tests were carried out to a maximum vertical pressure of 150kN/m^2. The friction resistance of the mud cake is expressed in terms of effective stress parameters, cohesion *c*' and internal friction angle ϕ'. It can be noted from Figure 2 that:

a) The frictional resistance of the mud cake formed of polymer slurry was by far larger than that of the cake formed of bentonite slurry,
b) For the mud cakes formed of bentonite slurry, the cohesion c' increased significantly with age but the friction angle ϕ' tended to drop gradually with age (time),
c) For the mud cakes formed of polymer slurry, the cohesion c' increased in the early age and remained constant regardless of the age (time).

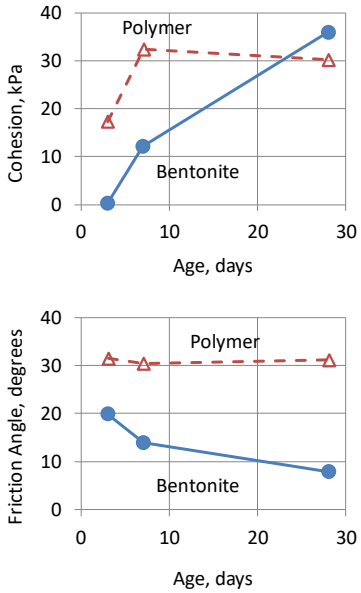

Figure 2 Time effects on shearing strengths of mud cakes formed of bentonite and polymer slurry time (Hosoi, T., 1993)

2.3 Mechanism of forming mud cakes

Polymer slurry is highly viscous and would not be able to infiltrate into soils with low permeability. Therefore the water contents in cakes surround by clayey soils would only be reduced slightly and the strengths of the cakes would hence be low. On the other hand, for cakes surrounded by sands, much slurry would infiltrate into the ground resulting in increase in densities and, hence, the strength of the cakes. In such cases, the slurry infiltrating into the sands would form a layer with characteristics very different from the characteristics of the remaining mud. This layer of mixture of sand and filtrate is called permeation deposit layer, and this phenomenon is called "standard plugging" in the filtration theory. If the permeability of the surrounding soils is uniform, the thickness of the cake would be more or less constant. Otherwise, the thickness of the cake would vary from place to place.

2.4 Thicknesses of cakes by API tests

The relationship between the thickness of cake and the elapsed time has been studied by many researchers and it has been found that:

1) The amount of slurry infiltrating into the ground under a constant pressure is theoretically proportional to the square root of the elapsed time. (Ruth's constant pressure filtration formula)
2) The thickness of the mud cakes can be calculated as follows.

$$f_c = \frac{w_l}{a(c_s / m_s - 1)} \qquad (1)$$

where,

f_c: *thickness of cake*
c_s: *volumetric concentration of solids in cake*
m_s: *volumetric concentration of solids in mud*
w_l: *amount of filtrate*
a: *filtration area*

The in-situ pressure in slurry varies depending on the depth, groundwater pressure, and the density of the slurry, and can be expressed by as follows:

$$p = 0.1\gamma(d - s_l) - (d - w_l) \qquad (2)$$

where,

w_l: *Groundwater level (m)*
γ: *Slurry density (kgf/cm²)*
s_l: *Slurry level (m)*
d: *Depth (m)*

The in-situ pressure should fall in the range of 25-50kN/m² under usual circumstance.

2.5 Management of slurry

As the shaft friction on barrettes and bored piles is closely related to the strength and the thickness of the mud cake formed at the interface between the piles and the ground, slurry has to be properly managed to serve its purpose. As shown in Table 2 and also Figure 3, model calculations indicate that the cake becomes significantly thicker as the density of the slurry increases. Figure 4 presents an example for determining the composition of the slurry from its density. Meanwhile, the thickness of the cake increases in proportion to the time period because the amount of filtrate increases in proportion to the square root of time.

Table 2 Composition of slurry and mud cakes

Slurry			Completely Full Filtration Case					
Density	Solid (kg)	Water (kg)	Mud Cake		At Full Filtration		Time Required (min)	
			Water (kg)	Volume (liter)	Water (liter)	Thickness (cm)	$\sqrt{T}$	T
1.020	32.1	987.9	25.7	37.8	962.2	3.8	473.3	223971
1.075	120.5	954.5	96.4	141.8	858.2	14.2	422.1	178171
1.100	160.6	939.4	128.5	189.1	810.9	18.9	398.9	159082
1.125	200.8	924.2	160.6	236.4	763.6	23.6	375.6	141075
1.150	240.9	909.1	192.7	283.6	716.4	28.4	352.3	124149
1.175	281.1	893.9	224.8	330.9	669.1	33.1	329.1	108305
1.200	321.2	878.8	257.0	378.2	621.8	37.8	305.8	93541

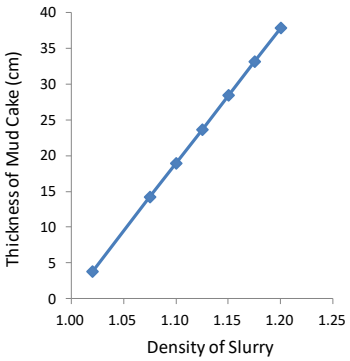

Figure 3 Relationship between the density of slurry and the thickness of mud cake

3. EFFECTS OF SHAPES OF PILES ON BEARING CAPACITY

3.1 Study 1: Circular piles versus rectangular piles

3.1.1 Full scale loading tests

Three sets of pile load tests were conducted on piles of 17.6 m, 22 m ad 20.25 m in length, with one barrette paired with one bored pile of almost the same sectional pile areas in each set. The geometry of these piles are depicted in Table 3 and Figure 5. These piles penetrated through a loam layer with SPT=10 to 15 and set in the underlying clay-mixed gravel layer with SPT >50.

【The component of mud】	Depth 20m
Density of soil particles	2.65
Density of bentonite	2.6
Density of polymer	1.5
Density of other additives	1.25
Mud density	1.180
Bentonite concentration	2%
Polymer concentration	0.30%
Other additives concentration	0.20%
Sand contents	3.00%
Conversion coeifficent to sand concentration	1.90
Mud volume	1,000 L

Component of mud	weight	volume
Water	888.3	888.3
Bentonite	17.8	6.8
Polymer	2.7	1.8
Additives	1.8	1.4
Mixed soil	269.5	101.7
Sumation	1180.0	1000.0
Segmentation of mixed soil particle size		
Clay and silty soil	212.5	80.2
Sandy soil	57.0	21.5

Over 15?m soil particles concentration	40.00%	
Weigt and volume after removal of over 15?m particles	weight 187.0	volume 70.6
Centrefuge treatment flow raio	30%	
Mud density after sand removal	***1.148***	
Mud density after centrifuge treatment	***1.133***	

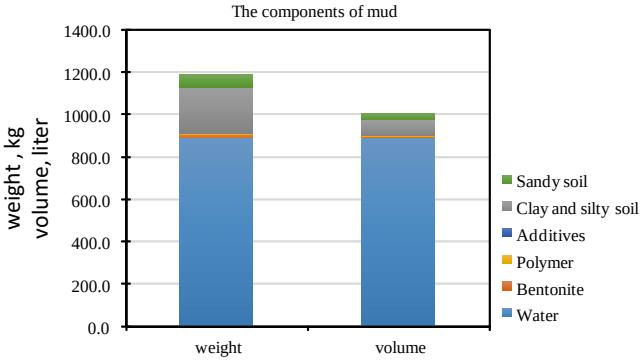

Figure 4 Example of composition of slurry

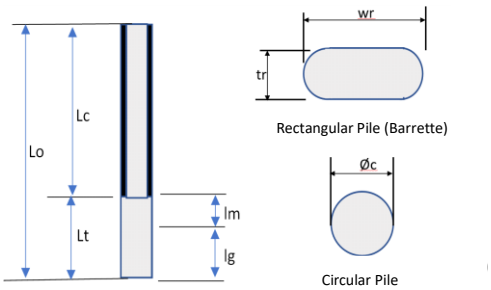

Figure 5 Definitions of the geometry of barrette and bored pile

Table 4 shows the results of tests and as can be noted, the skin friction and the end bearing capacity of barrette piles were greater than, or at least equal to, those of bored piles. The relationship between the applied load and settlement of the pile heads is illustrated in Figure 6. The barrettes (hollow symbols) obviously outperformed bored piles (solid symbols) with the same areas.

Table 3 Dimensions of full scale loading tests on barrettes and bored pile, Study 1
(Yamamoto, et al. 1983; Kimura, et al. 1983; Hosoi et al. 1994)

TEST NO	TEST PILE TOTAL LENGTH Lo(m)	FRICTION CUT LENGTH Lc(m)	TEST LENGTH (m)			FIRST YIELD LOAD (kN)		SKIN FICTION OF LOAM (kN/m2)		SKIN FICTION OF HARD GRAVEL LAYER WITH SPT >50(kN/m2)		RECTANGULAR PILE (BARRETTE PILE)		CIRCULAR PILE (BORED PILE)		
			Lt	lm	lg	BARRETTE PILE	BORED PILE	BARRETTE PILE	BORED PILE	BARRETTE PILE	BORED PILE	AREA Ar(m2)	PERIMETER Ur(m)	DIAMETER Øc(m)	AREA Ac(m2)	PERIMETER Uc(m)
TEST1	17.60	13.60	4.00	1.00	3.00	12000.00	8500.00	43.00	27.00	215.00	175.00	1.15	4.81	1.20	1.13	3.37
TEST2	22.00	17.00	5.00	2.50	2.50	12250.00	9250.00	121.00	117.00	214.00	210.00	1.15	4.81	1.20	1.13	3.37
TEST3	20.25	15.25	5.00	3.00	2.00	11000.00	10750.00	74.00	260.00	590.00	590.00	1.05	4.52	1.20	1.13	3.37

Table 4 Results of full scaled loading tests on barrettes and bored piles, Study 1

TEST NO	MAXIMUM TEST LOAD (kN)		FIRST YIELD LOAD (kN)		ULTIMATE BEARING CAPACITY(kN)		END BEARING CAPACITY AT FIRST YIELD LOAD (kN/m2)		SKIN FICTION OF HARD GRAVEL LAYER WITH SPT >50(kN/m2)	
	BARRETTE PILE	BORED PILE	BARRETTE PILE	BORED PILE	BARRETTE PILE	BORED PILE	BARRETTE PILE	BORED PILE	BARRETTE PILE	BORED PILE
TEST1	17000	13000	11000 - 13000	8000-9000	>17000	>13000	7560	5880	215 (at 73mm)	175 (at 75mm)
TEST2	18000	15000	12000-12500	9000-95000	28010 (Weibull Curve)	22380 (Weibull Curve)	7150	5750	214 (at 57mm)	210 (at 47mm)
TEST3	18000	18000	11000	10500-11000	22000 (Van der Veen)	20000 (Van der Veen	4465	3670	590	590

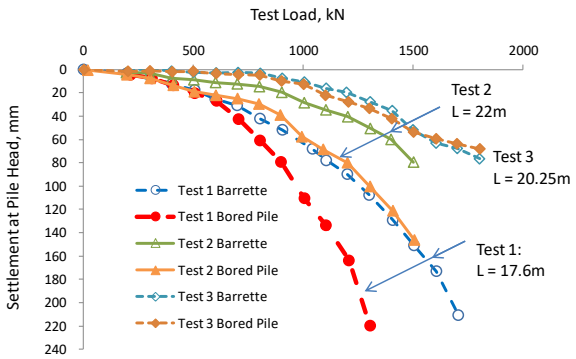

Figure 6 Relationship between pile settlements and loads, Study 1

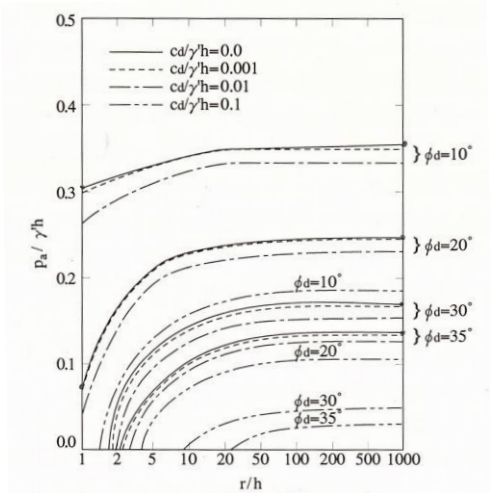

Figure 7 Earth pressures on piles as correlated with the aspect ratios of piles

3.1.2 Earth Pressures on pile shafts

The skin friction enveloped on the shafts of piles would depend on the earth pressures acting on the shafts. For simplicity, active earth pressures are assumed in the analyses. Active earth pressures, pa, acting on shafts are calculated by using the Generalized Limit Equilibrium Method (GLEM) proposed by Enoki et al (1991) and are normalized by the effective overburden pressure, γ'h , to correlate with the aspect ratios, *r/h*, of piles in Figure 7, where r = length of the longer side and h = length of the shorter side of piles. An aspect ratio of *r*/*h*=1.0 would refer to circular bored piles and an aspect ratio of *r*/*h*=1000 would refer to extremely thin (relative to the length) rectangular barrettes.

The curves shown in Figure 7 correspond to different $c_d/(rh)$ and ϕ_d values in which c_d is the drained shear strength of soil and ϕ_d = internal friction angle. The information given in Figure 7 is expressed in a different form in Figure 8. It can be noted from these two figures that the earth pressures acting on barrettes would be larger than those acting on bored piles of the same cross-sectional areas. This finding is in agreement with the fact that larger skin friction was obtained for the former than the later in the full scaled loading tests, refer to Table 3.

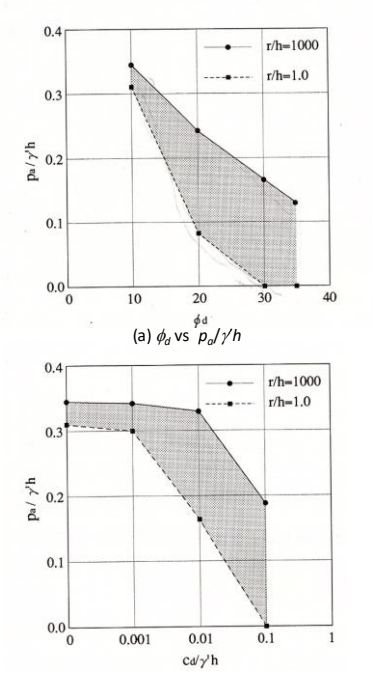

Figure 8 Active earth pressures on piles as affected by soil strength

3.2 Study 2: Flat piles versus nodular piles (Watanabe et al. 2012)

In recent years, a new type of foundation, i.e, nodular cast-in-place concrete piles with nodules at the middle sections of the piles as shown in Figure 9, has been developed to increase the load capacities of piles. In addition to larger load capacities, nodular piles have the advantages of lower costs and shorter construction periods in comparison with flat piles of the same cross-sections.

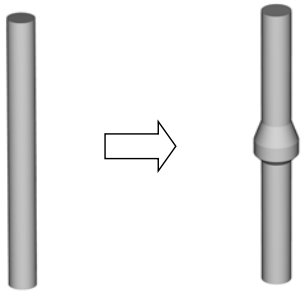

Figure 9 Schematic views of flat and nodular piles

To give an example, nodular piles were adopted to support a vibration control building in Osaka, Japan, and a pile load test was carried out to assess the performance of the piles. The test pile was 1m in diameter and 21 m in length with a nodule of 1.5 m in diameter at a depth of 9 m. The SPT N-value exceeds 50, as shown in Figure 10, at the depth of the nodule. The pile caps of the building foundation are founded at a depth of 6m (cap level) and therefore the shaft friction on the test pile above this depth was cut off by using an outer casing.

Compression load tests and tension load tests were carried out following JGS Standards (2002). For the tension load tests, 4 reaction piles were installed at distances larger than 3 times pile diameters away from the test pile to avoid interference to the performance of the test pile as shown in Figure 11. Since this paper focuses on the bearing capacity of piles, only compression load tests will be discussed hereinafter.

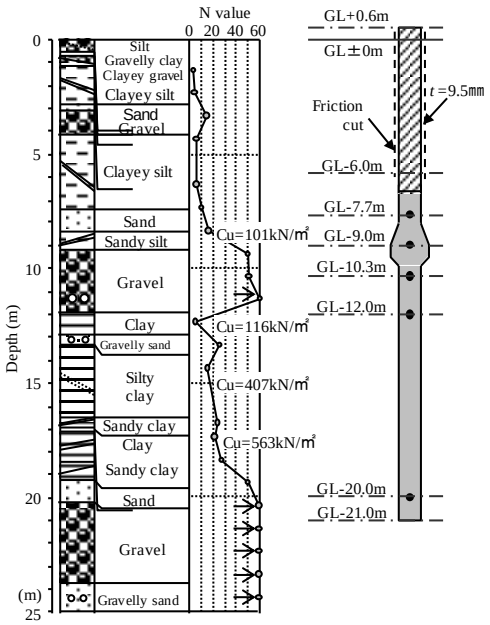

Figure 10 Soil profile and geometry of the test pile, Study 2

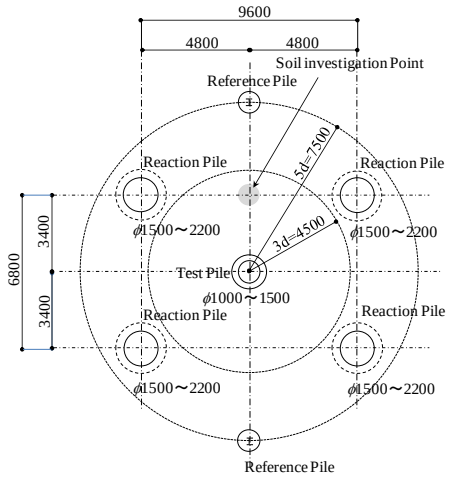

Figure 11 Layout of reaction piles in tension load tests, Study 2

To ensure that the pile was installed to the desired shape and dimensions, ultrasonic measurement was carried out and the results are shown in Figure 12. The images shown clear indicate that the pile was properly installed.

The compression load test was carried to a maximum load of 28,000kN in 8 steps as depicted in Figure 13. Loads applied were monitored by a load cell at the top of the pile and the strains induced in the shaft were monitored by strain gauges mounted on the rebars at 5 levels. Figure 14 shows the modulus of elasticity of concrete back calculated from the load applied and the strain measured.

The loads transferred to various depths are correlated with the displacement at the pile top in Figure 15. It can be noted that a maximum settlement of 175mm was observed at the top of the pile. The loads at the depth of pile cap, i.e., cap level, are correlated with the displacement at the top of pile in Figure 16.

Figure 17 shows the relationship between the shaft friction and the local pile displacement for each pile section of the pile. It can be noted that the shaft frictions in the gravel layer, ranging from depths of 10.3m to 12m, have not been fully mobilized while those in the underlying clay layers have reached their peak values.

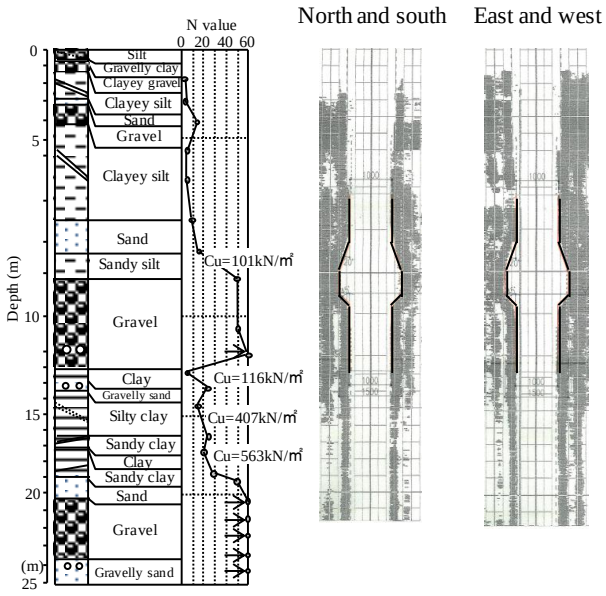

Figure 12 Ultrasonic measurement of the test pile, Study 2

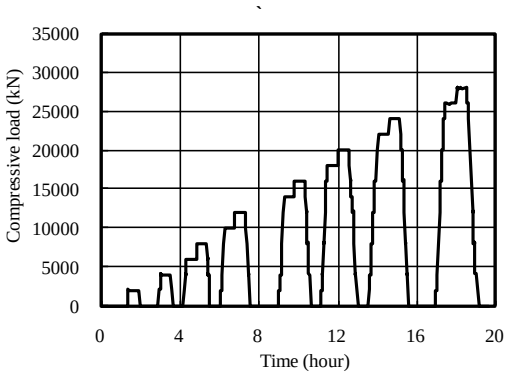

Figure 13 Loading sequence of compression loading test, Study 2

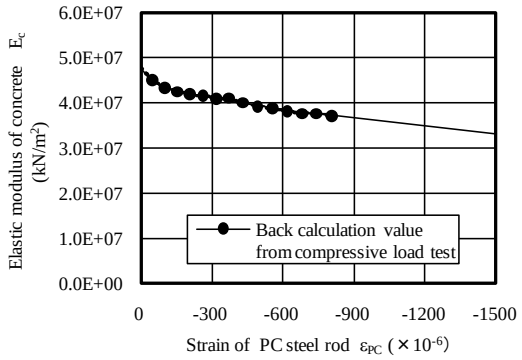

Figure 14 Modules of elasticity of concrete calculated from test results, Study 2

As illustrated in Figure 18, the load taken by the nodule equals the difference of loads above and below the nodule and the bearing pressures acting on the annulus at the base of the annulus equal the load taken by the nodule divided by the area of the annulus. Figure 19 shows the relationships between the bearing pressure acting on the nodule and local pile displacement as compared to the bearing pressures at the base of the pile. The bearing pressures reached 6,840 kPa on the nodule with a local displacement of 174 mm and 20,280 kPa at the base of the pile with a displacement of 166 mm. These bearing pressures did not reach their limits and tended to increase at the end of the test as depicted in the figure.

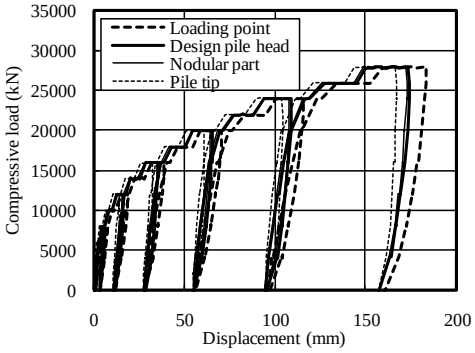

Figure 15 Settlements of piles at various depths, Study 2

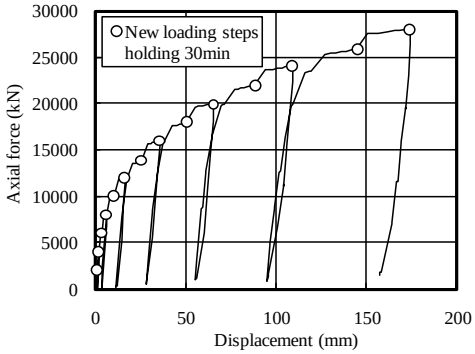

Figure 16 Settlements of the pile at the depth of design pile head, Study 2

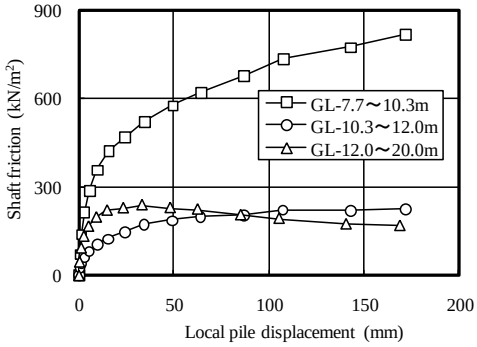

Figure 17 Shaft friction versus local displacements of piles, Study 2

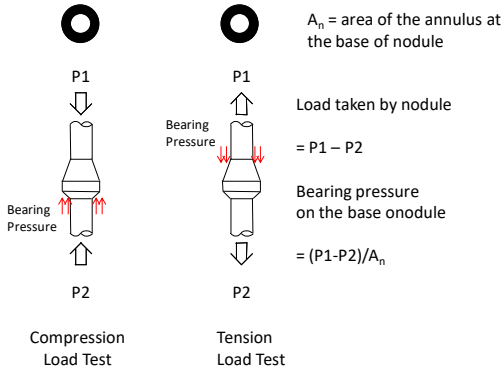

Figure 18 Compute the loads and bearing pressures on nodules

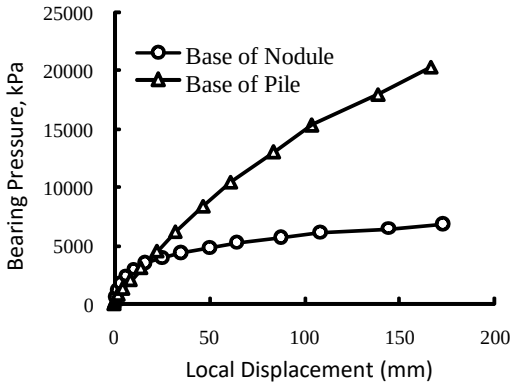

Figure 19 Bearing pressures on the nodule and the base of pile, Study 2

Many tests have been previously conducted on nodular piles. Based on the experience gained, Equations (3) and (4) are the empirical equations for the estimation of bearing pressure on nodules in sandy and clayey soils, respectively:

$$P_v = 100\ N \qquad P_v < 6{,}000\ kPa \qquad (3)$$

$$P_v = 6\ c_u \qquad Pv < 7{,}000kPa \qquad (4)$$

where,

p_v: *Bearing pressure on nodule (kN/m²)*

$\overline{N}$ *: Average SPT N value*

c_u: *Undrained shear strength (kPa)*

3.3 Study 3: Piles with nodules and under-reamed bases (Watanabe et al. 2011)

To assess the effectiveness of nodules in the increase of the capcities of piles, three piles were tested as follows, refer to Figure 20:

1) Flat circular bored pile
2) Nodular circular bored pile with under-reamed base, and
3) Nodular rectangular barrette with under-reamed base.

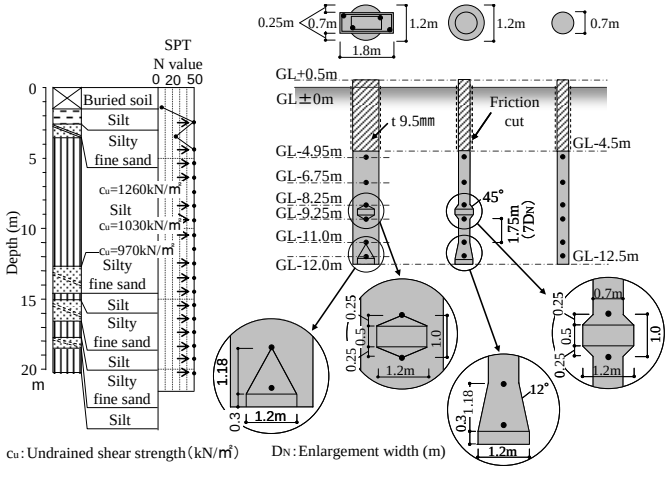

Figure 20 Soil profile and configurations of test piles with and without nodules, Study 3

Test Piles 1 and 2 were 0.7mm in diameter and Test Pile 3 was 0.7m in width and 1.8m in length. All these test piles went down to a depth of 12.5m below the ground surface and reached the top of the very dense silty sand layer as shown in Figure 20. Casings were installed to a depth of 5m to cut off shaft friction on all the three piles.

The soil profile given in Figure 20 shows that, the ground consists of fill (buried soil) at surface, hard silt and clayey sand at depth of 0~3.5m, consolidated silt with SPT N values exceeding 50 at depth 3.5m~12.5m, and very dense silty sand and very hard consolidated silt at the bottom of the log.

For Test Piles 2 and 3, the nodules were located at a depth of around 9m. The shapes and the sizes of the nodules and the under-reamed bases are depicted in Figure 20. The results of ultrasonic measurement shown in Figure 21 confirm that the two nodular piles were installed properly as desired. This is further confirmed by Photo 1 which shows Test Piles 2 and 3 after they were retrieved from the ground after tests.

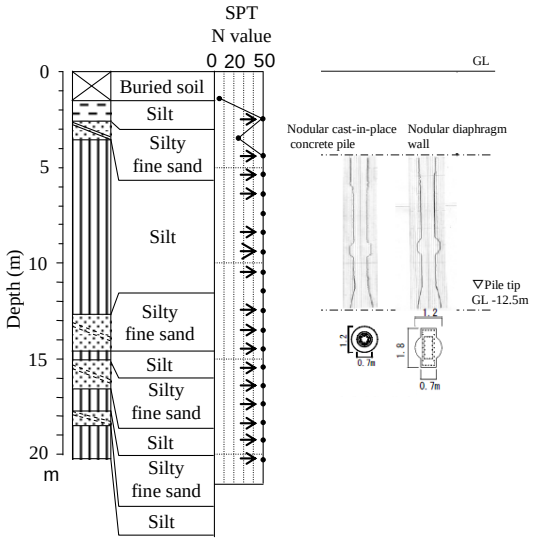

Figure 21 Results of ultrasonic measurement of the test pile, Study 3

Photo 1 Nodular bored pile ad nodular barrettes as they were retrieved from the ground, Study 3

Figure 22 shows the hysteretic load-displacement relationship obtained at the pile head. As can be noted, Pile 2 offered larger resistance against both compressive and tensional loads than Pile 1 for any given displacement, while pile 3 outperformed the other two. Figures 23 show similar relationship at a depth of 5m i.e., the bottom depth of the outer friction cutoff casings.

The relationships between the bearing pressures and displacements are show in Figures 24 and 25 for the nodules and the under-reamed bases of Piles 2 and 3, respectively. As can be noted, the bearing pressures on nodules did not reach their limit at the end of compression load tests on both piles. The bearing pressures at the enlarged bases are small in both cases because the movements of the bases were small.

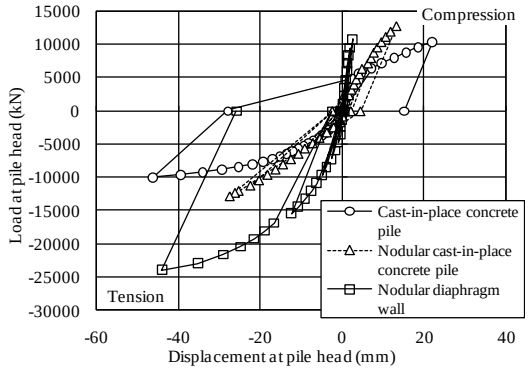

Figure 22 Relationship between settlements and loads of piles at pile heads, Study 3

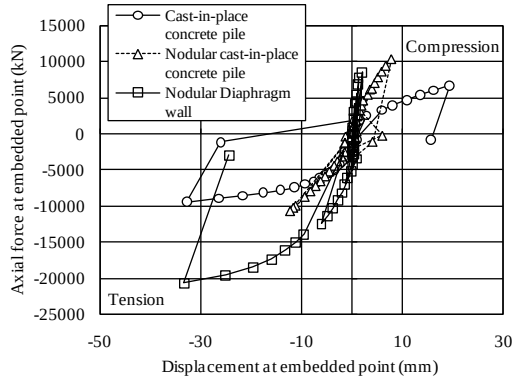

Figure 23 Relationship between axial forces and displacement at embedded point, Study 3

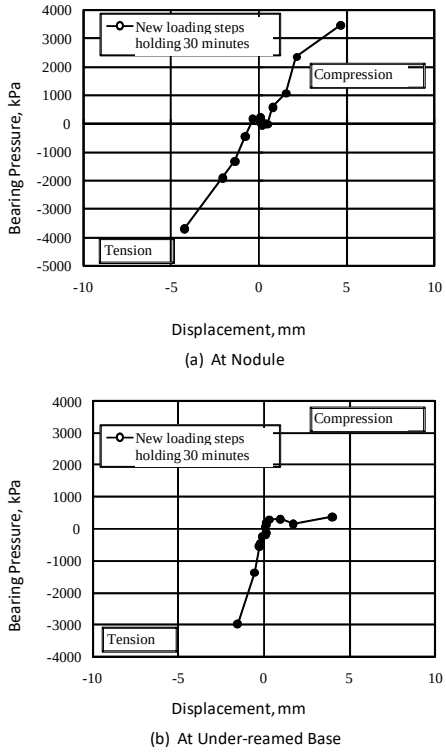

Figure 24 Relationship between bearing pressures and displacement on nodules of nodular piles, Study 3

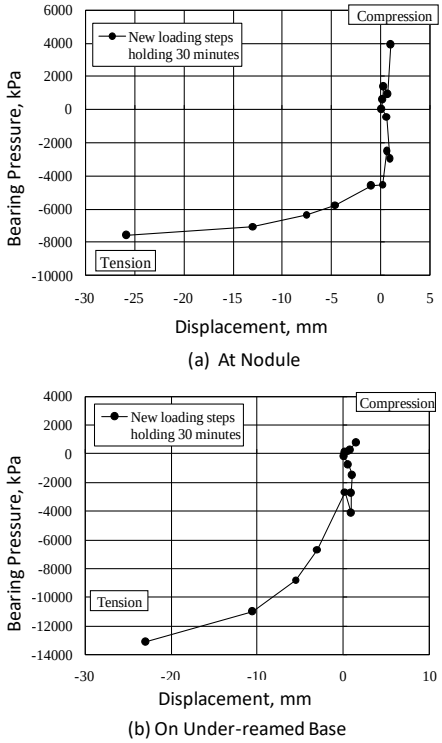

Figure 25 Relationship between bearing pressures and displacement on nodular barrettes, Study 3

4. MODULI OF ELASTICITY OF CONCRETE

4.1 Key Issues

The quality of concrete is doubtlessly a governing factor on the performance of piles: It is thus important to take the following issues into consideration in the interpretation of the results of load tests:

1) Concrete is cast into bored holes and/or trenches by using Tremie pipes and consolidated by its own weight. Although a vibrator is used for densifing concrete, the properties of concrete may vary from place to place. The example given in Figure 26 shows drastic variation of the strength and modulus of elasticity of concrete obtained in a test pile as evidenced by the scatter of data,
2) Inward movement of ground (bulging) and local collapse (necking) of excavated wall frequently occur, consequently, the sectional areas of test piles are not necessary constant.
3) To start with, as steel cages are very heavy, they are difficult to be positioned to the exact design levels, therefore the strain gauges mounted on rebars may be mislocated. The situation is worsen by the fact cages are dragged down as concrete is cast. Figure 27 shows an example in which the hauling load, including the weight of cage and the drag on the cage, of a re-bar cage for a 100m deep, 1.2m thick diaphragm wall panel reached as much as 500kN.
4) The modulus of elasticity of concrete will be different in compression load tests and tension load tests. In the later, tensional cracks may occur and the properties of concrete may be affected as a result.

4.2 Modulus of elasticity of concrete in compression load tests

In the static compressive load tests the pile axial loads at a section can generally be calculated from the readings obtained by the strain gauge mounted at the section as follows:

$$P_i = \varepsilon_i (E_{ci} \cdot A_{ci} + E_{si} \cdot A_{si}) \quad (5)$$

where,
P_i: *Axial load in pile at section I*
ε_i: *Strain at section I*
E_{ci}: *Modulus of elasticity of concrete*
A_{ci}: *Cross-section area of concrete*
E_{si}: *Young's Modulus of elasticity of steel bars*
A_{si}: *Cross-section area of steel bars*
Young's modulus of elasticity of rebars of various grades of steel, E_{si} , are usually given by steel manufactures. The modulus of elasticity of concrete (E_{ci}) can be estimated as follows;

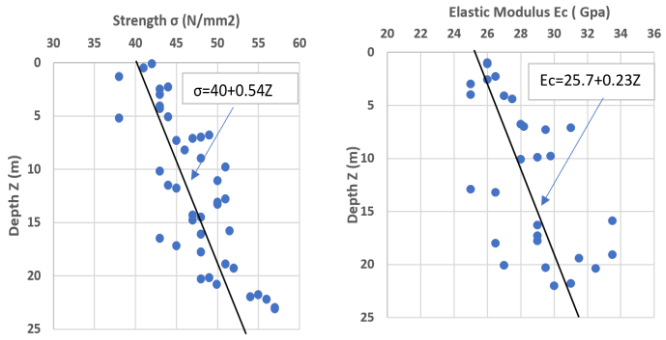

Figure 26 Strengths and moduli of elasticity of concrete at various depths

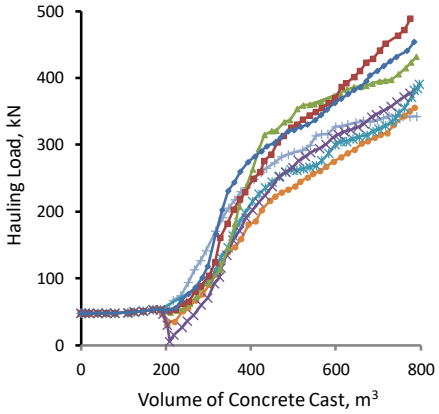

Figure 27 Drags on a steel cage during casting of concrete (Hosoi and Matsushita 2016

1) Method 1: Cube Test (fresh concrete cube or cores of test pile)
2) Method 2: Tangent modulus of elasticity
3) Method 3: Secant modulus of elasticity at upper strain gauges which are unaffected by the shaft resistance

In Method 1, the modulus of elasticity of concrete can be directly obtained from the tests.

In Method 2 and Method 3, the modulus of elasticity of concrete from pile load tests is given by Equation (6).

$$P_i = \varepsilon_i \cdot E_{csi} \cdot A_{csi} \quad (6)$$

where,
ε_i: *Strain at section I of the test pile*
E_{csi}: *Combined modulus of elasticity of elasticity of concrete and steel bars*
A_{csi}: *Combined area of concrete and steel bars at section i*

The modulus of elasticity of concrete is strain dependent. Assuming a linear relationship between the two, the following was proposed by Fellenius B. H. (2001) to evaluate the tangent modulus of elasticity of concrete (M_t) :

$$Mt = d\sigma / d\varepsilon = A\varepsilon + B \quad (7)$$

By integration, Equation (7) yields:

$$\sigma = (A/2)\varepsilon^2 + B\varepsilon + C \quad (8)$$

Constant C should be assumed zero, then

$$\sigma = (A/2)\varepsilon^2 + B\varepsilon \quad (9)$$

The secant modulus of elasticity of (E_{cs}) is defined as:

$$E_{cs} = \sigma / \varepsilon \quad (10)$$

and,

$$E_{cs} = (A/2)\varepsilon + B \quad (11)$$

where,
σ: *Test load divided by sectional area = stress*
ε: *Measured strain*
A: Slope of the modulus versus strain relationship
B: y-intercept of the modulus versus strain relationship

Instruments are frequently damaged and give misleading readings. For example, Figure 28 presents the results of a loading test on a pile of 1m in diameter and 27m in depth. The raw data obtained at a depth of approximate 20m are obviously erroneous. The strain gauges at this level could have been damaged, therefore, the readings obtained have to be somehow corrected to enable the performance of the pile to be reasonably interpreted.

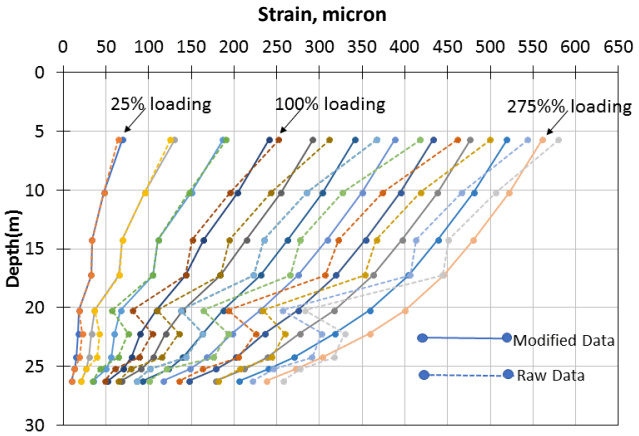

Figure 28 Stains at various depths, raw data and modified data

Figure 29 plots the tangent modulus of elasticity obtained based on the raw data given in Figure 28 before modification and the tangent modulus of elasticity of concrete can be correlated with the strain as follows:

$$Mt = -0.053\varepsilon + 73.83, \quad (12)$$

and the combined modulus of elasticity of concrete and rebars can be expressed as follows

$$Ecs = -0.0265\varepsilon + 73.83. \quad (13)$$

The readings can be adjusted based on the best engineering judgment as illustrated in Figure 28 and the tangential modulus are re-plotted in Figure 30. It then follows:

$$M_t = -0.0051\varepsilon + 52.77 \quad (14)$$

and,

$$E_{st} = -0.00255\varepsilon + 52.77 \quad (15)$$

As can be noted, the scatter of data is much less in Figure 30 than in Figure 29.

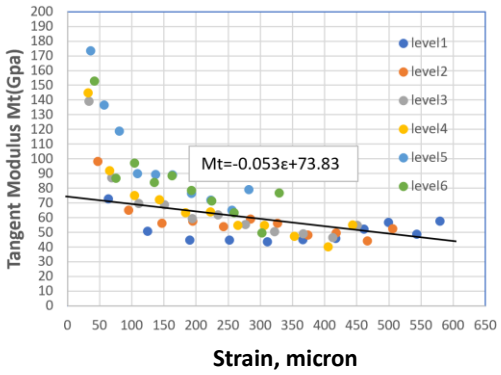

Figure 29 Tangent moduli of elasticity of concrete based on raw data

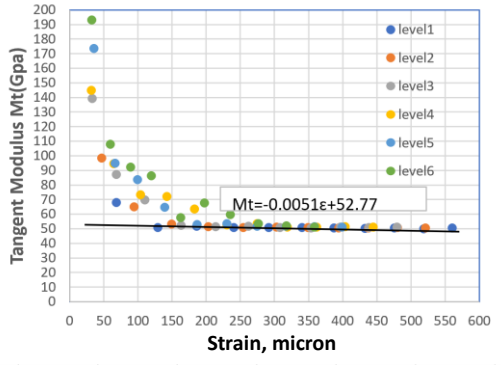

Figure 30 Tangent moduli of elasticity concrete based on modified data

For a maximum strain of 550 micros at peak load, refer to Figure 28, the tangent modulus of elasticity would be E_{cs}=59.3GPa based on raw data and M_t=51.4GPa based on the modified data. The difference between these two values is about 15%.

Method 3 is the most common method adopted and is specified as "Method for Static Axial Compressive Load Test of Single Piles (JGS1811-2022)" in the Japanese Pile Load Test Guidelines. The secant modulus of elasticity can be expressed, as depicted in Figure 31, as follows:

$$Est = -0.0125\varepsilon + 58.82 \ (GPa) \quad (16)$$

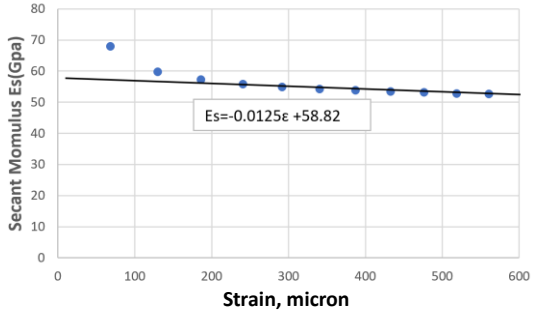

Figure 31 Secant moduli of elasticity of concrete base on modified top level data

At a maximum strain of 550, the Secant Modulus is about E_{cs}=52.0Gpa. The difference between E_{st} obtained by using Method 2 and Method 3 is 1%.

4.3 Moduli of elasticity of concrete in tension load tests

The mechanical properties of concrete are different in compression load tests and tension load tests. A tower of 634 m in height, for example, was constructed in 2012 to serve as an antenna tower for broadcast in Tokyo metropolitan area. Design of the foundation of the tower accounted for earthquake and wind loads and demanded tension load tests for assessing the capacity of the foundation against tension.

Two types of foundation were considered in the preliminary design: 1) Counter weight plan by open caisson method (Figure 32a) and, 2) Nodular SRC (Steel Reinforced Concrete) barrettes (Figure 32b). The latter is a newly developed type of foundation with nodules in the middle sections of the barrettes. For the former foundation type, it was envisaged that construction of the caissons would influence the operation of the existing railway nearby because the sinking of caissons by their own weights would drag the surrounding ground to sink together with the caissons. In contrast, ground settlements induced in the installation of barrettes would be minimal. Furthermore, this foundation type can reduce the construction cost and construction period compared to the former.

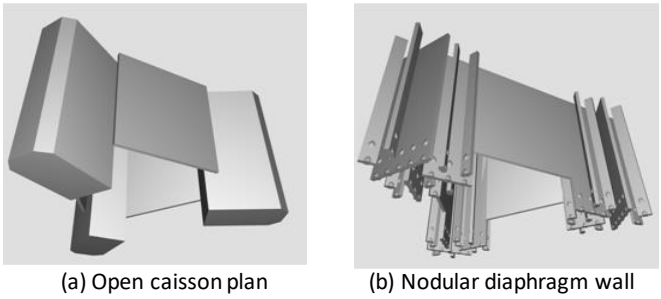

Figure 32 Options of foundation types, Tokyo Broadcasting

Nodular barrettes were finally adopted. They were 20 m in width, 1.2 m in thickness and 45 m in depth. Load tests on a full-size barrette were practically impossible because of the magnitudes of the test loads required. Accordingly, load tests were carried out on a nodular barrette reduced to 4 m width, 1.2 m thick and 45 m deep. The layout of reaction piles is depicted in Figure 33.

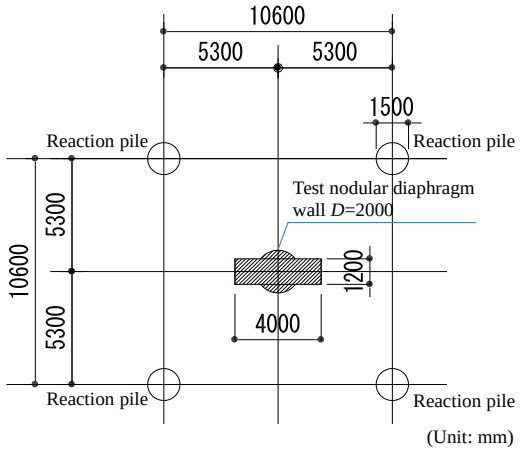

Figure 33 Layout of test barrette and reaction piles in tension loading test, Tokyo Broadcasting

With a design tension load of 36 MN, tests were carried out to a maximum load of 43MN which is 1.2 time the design load. To increase the load capacity, a nodule is located at a depth of 40 m, where SPT N-values exceed 40 as depicted in Figure 34. The base of the barrette was embedded in the gravel layer at a depth of 44.5 m below ground surface and was under reamed. The shaft friction above a depth of 10m, which is the design depth of pile capes, was cut off by using an outer casing.

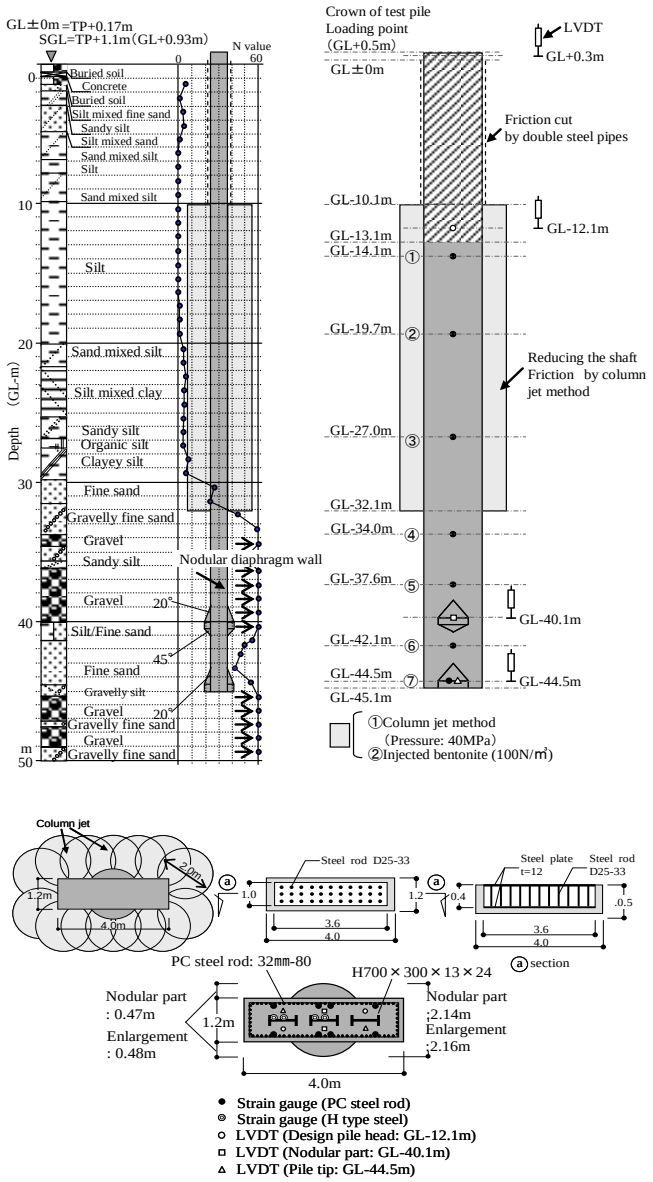

Figure 34 Soil profile and geometry of the test barrette, Tokyo Broadcasting

Naganuma and Yamaguchi (1990) reported the softening characteristics of concrete in tension loading. The cyclic behavior of reinforced concrete was also summarized by Naganuma and Ohkubo (2000). Based on these works, the relationship between tensile stress and tensile strain was estimated as shown in Figure 35. The tensile stress (or force) induced in the test barrette was estimated from the measured strain using the stress-strain relationship given in the figure. The relation indicated by the solid line was used for new loading steps, while the relations indicated by the dashed lines were used for repeated loading steps.

Figure 36 shows the relationship between the tensile load and displacements at the pile top (the loading point), the design pile head (i.e., depth of 10m), the nodule (depth of 40.1m) and the base (depth of 44.5m). Figure 37 shows the paths of tensile loads and displacements at the design wall head in every cycle of loading. It is inferred from Figure 37 that the capacity of the pile would certainly excess 40 MN.

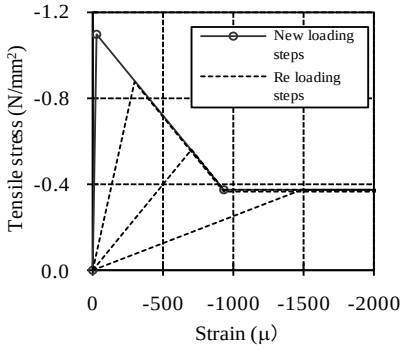

Figure 35 Relationship between stresses and strains of concrete

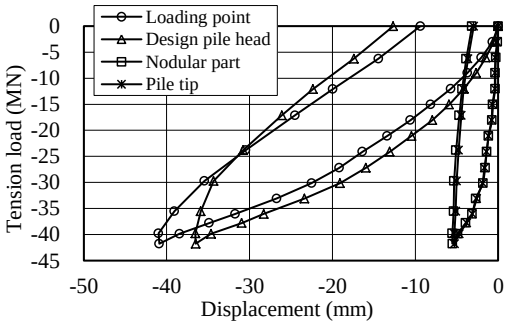

Figure 36 Relationship between the tensile loads and displacement at loading point, 1st load test, Tokyo Broadcasting

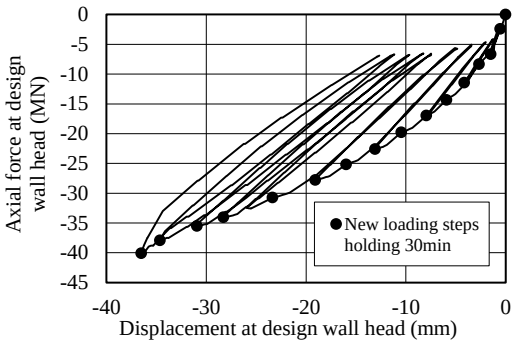

Figure 37 Relation between axial force and displacement at design pile head, 1st load test, Tokyo Broadcasting

It can be noted from Figure 38 that the shaft friction to a depth of 34 m was fully mobilized while the shaft friction below this depth did not reach their limits. As shown in Figure 39, the bearing pressures, p_v, of the nodule and the under-reamed base of pile reached 5,800kN/m^2 and 1,500kN/m^2 at displacements of 5.5 and 5.3 mm, respectively. These bearing pressures did not reach their ultimate values as depicted in the figure. In order to obtain the ultimate values of p_v , a second tension load test was carried out and the shaft friction was cut off to a depth of 32.1m by using the column jet technique (see Figure 34).

The test was carried out to the same load, i.e., 42 MN, as the first test. The relationships between bearing pressure and displacement in the second tension load test are shown in Figure 40. The bearing pressures exceeded their limits at the nodule and at under-reamed base. The bearing pressures at peak load are 6,450kN/m^2 for a displacement of 29mm at the nodule and 3,000kN/m^2 for a displacement of 19mm at the base.

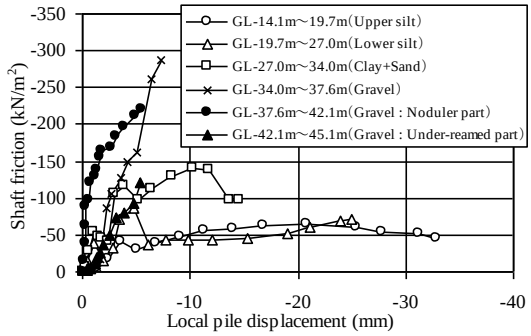

Figure 38 Relationship between shaft frictions and local pile displacements, 1st load test, Tokyo Broadcasting

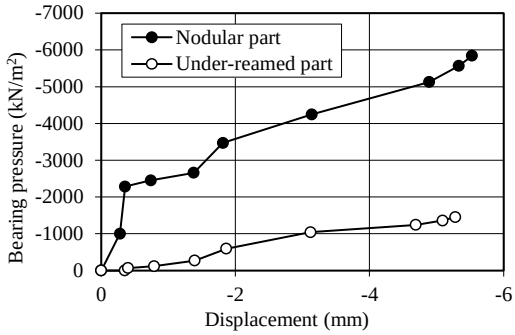

Figure 39 Relationship between bearing pressures and displacements, 1st load test, Tokyo Broadcasting

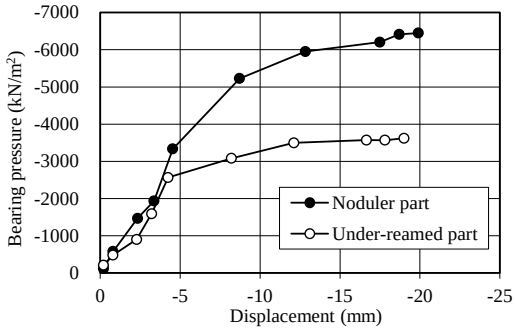

Figure 40 Relationship between bearing pressure and displacement, 2nd load test, Tokyo Broadcasting

5. CONCLUSIONS

The foregoing discussions lead to the following conclusions:

1) The strength and thickness of mud cake are important factors affecting the shaft friction of piles. The results obtained from the laboratory test carried out in this study, as depicted in Figures 2 and 3 will be useful in assessing the strengths and thicknesses of cakes.
2) The results of load tests indicate the capacities of barrettes are in general larger that the capacities of bored piles with the same cross-sectional areas.
3) The capacities of piles can be increased by making piles nodular and/or by under-reaming the bases of piles.
4) The moduli of elasticity of concrete can obtained from the forces and strains measured in pile load tests and the methods presented herein will be useful.

6. REFERENCES

Carlos, L., and Stephan, A. J., (2014) "The use of polymer solutions for deep excavations: lessons from Far Eastern experience", HKIE Transactions 2014, Vol21, No4, pp262-271.

Fellenius, B. H., (2001) "From Strain Measurements to Load in an Instrumented Pile", Geotechnical News Magazine,Vol 19, No.1, pp35-38.

Hosoi, T. (1993) "Bearing capacity of diaphragm wall foundation and various issues during its construction". Doctoral Thesis, Kyoto University, pp79-88. (in Japanese)

Hosoi, T. and Matsushita, S., (2016) "Recent Diaphragm Wall Technologies and Future Challenge", Geotechnical Engineering Journal of the SEAGS & AGSSEA, Vol47, No2, pp118-120.

Naganuma, K. and Yamaguchi, T., (1990) "Tension Stiffening Model under In-plane Shear Stress", Proceedings of Annual National Conference on Architectural Institute of Japan, pp649-650. (in Japanese)

Naganuma, K. and Ohkubo, M., (2000) "An Analytical Model for Reinforced Concrete Panels under Cyclic Stresses", Journal of Structural Const. Engineering, Architecture Institute of Japan, No. 536, pp135-142. (in Japanese)

The Japanese Geotechnical Society (2002) "JGS standard, Method for Axial Load Test of Single Piles". (in Japanese)

Watanabe, K., Sudo, T., Nshimura, K. and Ishii, Y,, (2012) "In-situ Static Axial Load Tests of Nodular Cast-in-place Concrete Pile and Estimation Method on Resistance of Nodular Part", Proceedings of 9th International Conference on Testing and Design Methods for Deep Foundations (Kanazawa), pp749-756.

Watanabe, K., Sudo, T., Sato, M. and Ishii, Y., (2015) "Static Load Tests of Nodular Diaphragm Wall Supporting High-rise Tower", Proceedings of 15th Asian Regional Conference.